RESEARCH PAPER

Channels 7:3, 171–181; May/June 2013; © 2013 Landes Bioscience

Developmental alterations in the biophysical properties of $Ca_v1.3$ Ca^{2+} channels in mouse inner hair cells

Akira Inagaki and Amy Lee*

Departments of Molecular Physiology and Biophysics, Otolaryngology - Head and Neck Surgery and Neurology; University of Iowa; Iowa City, IA USA

Keywords: inner hair cell, Ca^{2+} channel, calmodulin

Prior to hearing onset, spontaneous action potentials activate voltage-gated $Ca_v1.3$ Ca^{2+} channels in mouse inner hair cells (IHCs), which triggers exocytosis of glutamate and excitation of afferent neurons. In mature IHCs, $Ca_v1.3$ channels open in response to evoked receptor potentials, causing graded changes in exocytosis required for accurate sound transmission. Developmental alterations in $Ca_v1.3$ properties may support distinct roles of $Ca_v1.3$ in IHCs in immature and mature IHCs, and have been reported in various species. It is not known whether such changes in $Ca_v1.3$ properties occur in mouse IHCs, but this knowledge is necessary for understanding the roles of $Ca_v1.3$ in developing and mature IHCs. Here, we describe age-dependent differences in the biophysical properties of $Ca_v1.3$ channels in mouse IHCs. In mature IHCs, $Ca_v1.3$ channels activate more rapidly and exhibit greater Ca^{2+}-dependent inactivation (CDI) than in immature IHCs. Consistent with the properties of $Ca_v1.3$ channels in heterologous expression systems, CDI in mature IHCs is not affected by increasing intracellular Ca^{2+} buffering strength. However, CDI in immature IHCs is significantly reduced by strong intracellular Ca^{2+} buffering, which both slows the onset of, and accelerates recovery from, inactivation. These results signify a developmental decline in the sensitivity of CDI to global elevations in Ca^{2+}, which restricts negative feedback regulation of $Ca_v1.3$ channels to incoming Ca^{2+} ions in mature IHCs. Together with faster $Ca_v1.3$ activation kinetics, increased reliance of $Ca_v1.3$ CDI on local Ca^{2+} may sharpen presynaptic Ca^{2+} signals and improve temporal aspects of sound coding in mature IHCs.

Introduction

Voltage-gated Ca_v Ca^{2+} channels conduct inward Ca^{2+} currents that can depolarize the membrane potential and trigger Ca^{2+}-dependent signal transduction in excitable cells. Multiple classes of Ca_v channels ($Ca_v1.x$-$Ca_v3.x$) have been characterized,[1] which play distinct roles often within the same cell. In most neurons, somatodendritic Ca_v1 channels mediate L-type Ca^{2+} currents that couple neuronal activity to changes in gene transcription,[2,3] while presynaptic Ca_v2 channels generating P/Q- and N-type Ca^{2+} currents regulate neurotransmitter release from nerve terminals.[4-6]

In contrast to the diverse complement of Ca_v channnels in most neuronal cell-types, auditory hair cells express predominantly $Ca_v1.3$ channels, which mediate exocytosis of glutamate at ribbon synapses formed with primary afferent neurons.[7,8] Genetic inactivation of *CACNA1D* ($Ca_v1.3$ KO), which encodes the pore-forming α_1 subunit of $Ca_v1.3$, causes ~90% reduction in the whole-cell Ca^{2+} current in mouse inner hair cells (IHCs).[9-11] As a consequence, stimulus-secretion coupling is significantly impaired in $Ca_v1.3$ KO IHCs,[11] which contributes to deafness in these mice.[9,10] Spontaneous Ca^{2+}-dependent action potentials, which support presensory afferent synaptic transmission,[12-14] are absent in $Ca_v1.3$ KO IHCs. The developmental upregulation of BK K^+ channels and pruning of cholinergic efferents from the basal IHC membrane, which normally occurs around the onset of hearing,[13,15] are also absent in $Ca_v1.3$ KO IHCs.[11,16] Thus, $Ca_v1.3$ channels play distinct roles in regulating electrical activity and normal developmental programs in immature IHCs, and in transducing stimulus-evoked exocytosis in mature IHCs.

Comparisons of Ca_v1 currents in mature and immature auditory hair cells suggest differences in the properties of $Ca_v1.3$ channels that may tailor Ca^{2+} signals according to developmental stage. For example, in gerbil and rat IHCs, the extent to which Ca_v1 channels undergo Ca^{2+}-dependent inactivation (CDI) declines after hearing onset.[17,18] CDI is a negative feedback regulation of Ca_v1 and Ca_v2 channels by incoming Ca^{2+} ions, which depends on calmodulin binding to the Ca_v α_1 subunit.[19,20] CDI is relatively weak for Ca_v1 channels in IHCs, which may be due to the antagonistic actions of calmodulin-like Ca^{2+} binding proteins expressed in IHCs.[17,21,22] The rates of Ca_v1 channel activation and inactivation can significantly influence IHC Ca^{2+} signals that regulate presensory action potentials or stimulus-secretion coupling. Whether $Ca_v1.3$ channels in mouse IHCs

*Correspondence to: Amy Lee; Email: amy-lee@uiowa.edu
Submitted: 01/30/13; Revised: 02/23/13; Accepted: 02/25/13
http://dx.doi.org/10.4161/chan.24104

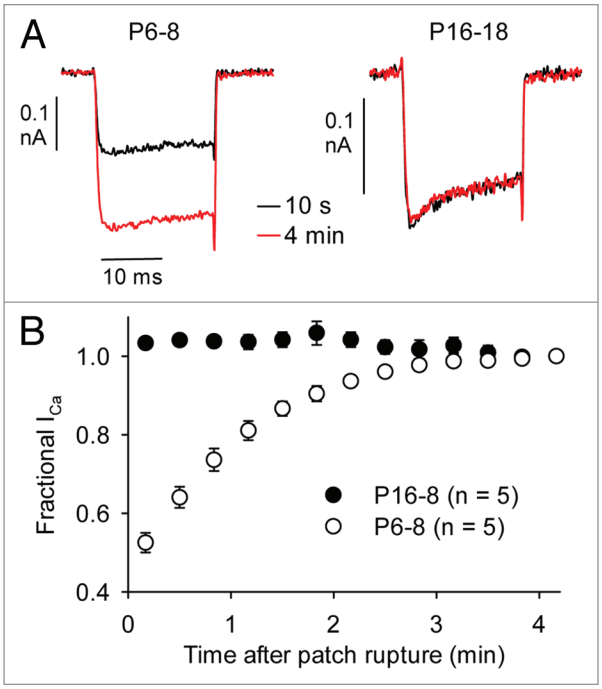

Figure 1. Run-up of I_{Ca} in immature mouse IHCs. (**A**) Representative current traces for I_{Ca} evoked by 20-ms test pulses to +10 mV, 10 sec and ~4 min after patch rupture. (**B**) I_{Ca} was normalized to that at 4 min after patch rupture and plotted against time.

undergo developmental changes in their biophysical properties is incompletely characterized. Given the widespread use of mice as experimental models for IHC transmission, filling this void is essential for understanding Ca^{2+}-dependent signaling in IHCs in this species.

In this study, we compared the properties of Ca^{2+} and Ba^{2+} currents (I_{Ca} and I_{Ba}, respectively) in IHCs from mice before and after hearing onset (~P12). We discovered that $Ca_v1.3$ channels exhibit significant differences in immature (P6–8) and mature (P16–18) IHCs in terms of activation and inactivation. In particular, CDI differs in magnitude and sensitivity to local rather than global Ca^{2+} elevations in Ca^{2+}. Our results highlight age-dependent distinctions in the properties of $Ca_v1.3$ channels that may fine-tune Ca^{2+} signals required for the development and mature function of IHCs.

Results

$Ca_v1.3$ currents activate with faster kinetics in mature IHCs than in immature IHCs. Because a goal of this study was to compare CDI before and after hearing onset in mouse IHCs, we first analyzed activation of both I_{Ca} and I_{Ba} in P6–8 and P16–18 mouse IHCs. Whole-cell patch clamp recordings were performed at room temperature in solutions designed to isolate $Ca_v1.3$ currents from other ionic currents, particularly voltage-gated K^+ currents (see *Materials and Methods*). The intracellular solution contained 2 mM EGTA, which is permissive for measuring CDI in IHCs.[17,18] Relatively high concentrations of extracellular Ca^{2+} or Ba^{2+} were used (5 mM) to amplify current amplitudes, thus increasing resolution of activation and inactivation kinetics. Consistent with previous studies of Ca_v1 channels in other cell-types,[23] I_{Ca} underwent a progressive increase in amplitude (run-up) upon attaining whole-cell configuration in immature IHCs (**Fig. 1**). For this reason, we first monitored the amplitude of I_{Ca} evoked by steps to +10 mV every 20 sec until there was no further run-up. Interestingly, run-up was not observed in mature IHCs, which was confirmed by the same protocol. Thus, data were collected ~5 min after whole cell patch rupture in immature IHCs, when steady-state I_{Ca} amplitudes were achieved. In mature IHCs, data were collected ~1 min after patch rupture to ensure equilibration with intracellular solution components.

As noted previously,[11,14] the most dramatic difference in $Ca_v1.3$ currents was the smaller amplitude of I_{Ca} and I_{Ba} in mature IHCs compared with immature IHCs. In current-voltage (I-V) relationships, the maximum current amplitude was obtained with a –10-mV pulse for I_{Ca} and was significantly smaller in mature IHCs than in immature IHCs (19.4 ± 15.4%; **Fig. 2A–D**). A similar difference was observed for I_{Ba} (32.9 ± 10.2%) except that the peak I_{Ba} was obtained between –10 and –0 mV, due to changes in surface charge screening when Ba^{2+} rather than Ca^{2+} is used as the permeant ion.[24] As has been reported for $Ca_v1.3$ in heterologous expression systems,[25] there was some rectification in the I-V relationship at positive voltages, probably due to limited permeability of $Ca_v1.3$ channels to Cs^+ ions. Thus for greater accuracy, we measured parameters for voltage-dependent activation in normalized tail current-voltage relationships fit with the Boltzmann equation. By this analysis, the voltage for half-maximal activation (V_h) was more positive and there was a significant increase in the slope factor (k) with age for I_{Ca} and I_{Ba} (**Table 1**; **Fig. 2E and F**). In addition, the activation kinetics of I_{Ca} were significantly faster in mature IHCs than in immature IHCs (~5–29% from –40 to +40 mV, $p < 0.001$ by two-way ANOVA; **Fig. 3A**). The acceleration in $Ca_v1.3$ activation depended on Ca^{2+} as the charge carrier since it was not observed for I_{Ba} ($p = 0.34$ by two-way ANOVA; **Fig. 3B**). These results indicate that, in addition to a reduction in $Ca_v1.3$ current density, the intrinsic biophysical properties of $Ca_v1.3$ channels also change with development.

Ca^{2+}-dependent inactivation is greater in mature IHCs than immature IHCs. To determine if $Ca_v1.3$ inactivation was also subject to developmental regulation in mouse IHCs, we compared the extent to which I_{Ca} and I_{Ba} inactivated in response to sustained depolarizations. Like other Ca_v1 channels, $Ca_v1.3$ undergoes inactivation due to Ca^{2+}- or voltage-dependent mechanisms (CDI and VDI, respectively). CDI manifests as stronger inactivation of I_{Ca} compared with I_{Ba}, due to Ca^{2+} binding to the calmodulin that is associated with the channel protein.[20] Unlike I_{Ca}, which undergoes both CDI and VDI, I_{Ba} exhibits purely VDI since Ba^{2+} substitutes poorly for Ca^{2+} in binding to calmodulin.[26] We measured CDI and VDI with a triple-pulse voltage-protocol in which I_{Ca} or I_{Ba} was evoked by test pulses before (p1) and after (p2) a 200-ms prepulse to varying voltages. Inactivation was measured as the ratio of the p2/p1 current amplitudes; this ratio was less than 1 for prepulses inducing inactivation (**Fig. 4A and B**). As expected for CDI, the prepulse-voltage dependence of I_{Ca} inactivation was U-shaped and was greatest for prepulses evoking the

maximal inward I_{Ca}. In contrast, inactivation of I_{Ba} with this protocol was not evident across the full prepulse voltage range. In mature IHCs, I_{Ba} underwent facilitation (p2/p1 > 1) at positive prepulse voltages, likely due to voltage-dependent facilitation (VDF).[27] Since I_{Ca} is thought to undergo VDI as well as VDF, we isolated the effects of CDI on I_{Ca} as the difference in p2/p1 for I_{Ca} and I_{Ba} (F_{CDI}, **Figure 4C**). By this metric, CDI was significantly greater in mature IHCs than in immature IHCs ($p < 0.001$ by two-way ANOVA).

To address the underlying mechanism(s) for the age-dependent increase in CDI, we analyzed the onset of I_{Ca} inactivation by obtaining p2/p1 ratios in voltage protocols with prepulses of varying duration (**Fig. 5A**). The prepulse was set to –20 mV for I_{Ca} and –30 mV for I_{Ba}, to partially compensate for the negative shift in activation voltages for I_{Ba} compared with I_{Ca} (**Table 1**). The duration of the p1 and p2 test pulse was increased to 5 ms in these experiments to ensure that test currents reached steady-state levels, as long prepulses tended to slow the activation kinetics of the p2 current. The onset of inactivation was obtained by plotting p2/p1 ratios for I_{Ca} against prepulse duration. With this protocol, I_{Ca} inactivated with a double exponential time course in both immature and mature IHCs. Both fast and slow inactivation were likely influenced by CDI: the fast component was not observed for I_{Ba}, and the slow component of I_{Ca} inactivation was significantly faster than that for I_{Ba} (τ_{slow} 2.0 ± 0.4 sec for I_{Ca} vs. 3.1 ± 0.6 sec for I_{Ba}, P6–8, $p = 0.15$; τ_{slow} = 0.8 ± 0.13 sec for I_{Ca} vs. 2.3 ± 0.4 sec for I_{Ba}, P16–18, $p < 0.001$; both by t-test). While there was no age-dependent difference in the time constants for I_{Ba} inactivation ($p = 0.3$), both the slow and fast time constants were significantly faster for I_{Ca} inactivation in mature IHCs than in immature IHCs (**Fig. 5C**, $p < 0.05$). However, the amplitudes of the slow and fast components of I_{Ca} inactivation did not vary with age (A_{fast} = –0.25 ± 0.01 for P6–8 vs. –0.23 ± 0.02 for P16–18, $p = 0.20$; A_{slow} = –0.40 ± 0.03 for P6–8 vs. –0.34 ± 0.01 for P16–18, $p = 0.31$; both by t-test). These results indicate that CDI is governed by fast and slow processes, both of which occur more rapidly in mature IHCs compared with in immature IHCs.

To analyze recovery from inactivation, p2 test currents were measured at varying intervals after the inactivating prepulse and the ratio of p2/p1 plotted against the recovery interval (**Fig. 6A**). The duration of the prepulse was limited to 200 ms since longer prepulses induced VDI, particularly in mature IHCs (**Fig. 5A**); this would complicate analyses of recovery from CDI. In single exponential fits of these data, there was no difference in the amplitude (A = 0.32 ± 0.02 for P6–8 vs. 0.37 ± 0.03 for P16–18, $p = 0.40$, by t-test) or time constant (τ = 425.9 ± 28.3 ms for P6–8 vs. 486.4 ± 87.7 ms for P16–18, $p = 0.08$, by Mann-Whitney rank sum test; **Fig. 6B**). These results indicate that greater CDI in mature IHCs results primarily from faster onset, rather than slower recovery, of I_{Ca} from inactivation.

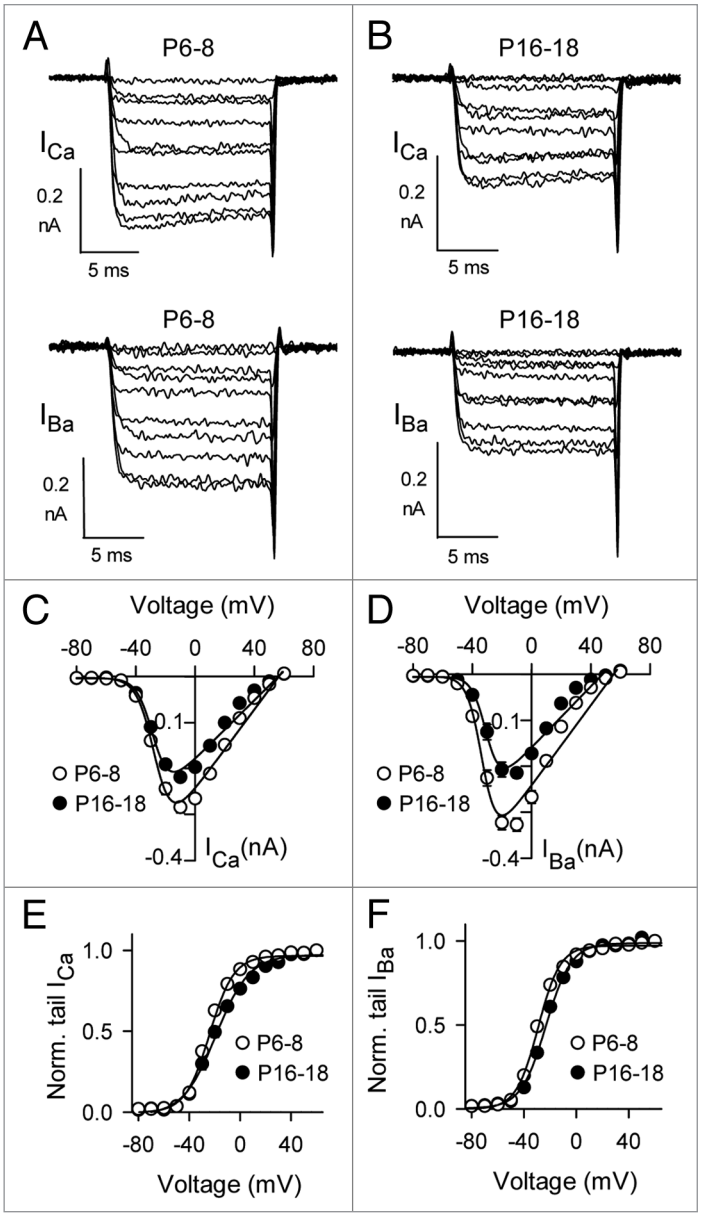

Figure 2. Voltage-dependent properties of I_{Ca} and I_{Ba} in mature IHCs and in immature IHCs. (**A and B**) Representative I_{Ca} (upper panels) and I_{Ba} (lower panels). Currents were evoked by 15-ms depolarizing pulses from a holding voltage of –84 mV. (**C and D**) I-V relationships for currents in (**A**). (**E and F**) G-V relationships for currents in (**A and B**). Tail current amplitudes were normalized to that obtained with a pulse to +50 mV (Norm. tail) and plotted against test voltage. Smooth lines in (**C–F**) represent curve fits from the Boltzmann equation. The parameters for the fits shown were: in (**C**), V_h = -26.6, k = -5.9, V_{rev} = 56.4 mV, G_{max} = 4.3 nS for P6–8 (n = 22), V_h = -27.7, k = -5.4, V_{rev} = 56.1 mV, G_{max} = 3.2 nS for P16–18 (n = 15); in (**D**), V_h = -32.8, k = -4.9, V_{rev} = 55.5 mV, G_{max} = 4.3 for P6–8 (n = 22), V_h = -30.1 mV, k = -4.7, V_{rev} = 48.0 mV, G_{max} = 3.3 for P16–18 (n = 15); in (**E**), V_h = -24.1 mV, k = 9.5 for P6–8 (n = 22), V_h = -19.0 mV, k = 13.1 for P16–18 (n = 9); in (**F**), V_h = -29.2 mV, k = 8.4 for P6–8 (n = 11), V_h = -23.2 mV, k = 9.6 for P16–18 (n = 15).

Ca^{2+}-dependent inactivation depends on local Ca^{2+} in mature IHCs but not immature IHCs. In heterologous expression systems, CDI of Ca_v1 channels is not affected by relatively high concentrations of intracellular Ca^{2+} buffers (i.e., 10 mM BAPTA), due to a reliance on rapid, local Ca^{2+} influx through individual channels.[28] However, CDI of Ca_v1 currents in

Table 1. Parameters for voltage-dependent activation of $Ca_v1.3$ currents in mouse IHCs

		P6–8	n	P16–18	n	*p* value[1]
I_{Ca} (2 mM EGTA)	Peak current density[2] (pA/pF)	–35.6 ± 1.8 (at –10 mV)	22	–23.0 ± 1.2 (at –10 mV)	15	< 0.001
	$V_{1/2}$ (mV)[3]	–24.1 ± 0.9		–19.0 ± 1.8	9	0.009
	k[3]	9.5 ± 0.3		13.1 ± 0.7		< 0.001
I_{Ba} (2 mM EGTA)	Peak current density[2] (pA/pF)	–36.2 ± 1.8 (at –10mV)	11	–21.7 ± 1.2 (at –10mV)	15	< 0.001
	$V_{1/2}$ (mV)[3]	–29.2 ± 1.1		–23.2 ± 0.9		< 0.001
	k[3]	8.4 ± 0.3		9.6 ± 0.3		0.011
I_{Ca} (10 mM BAPTA)	Peak current density[2] (pA/pF)	–34.5 ± 1.3 (at –10 mV)	25	–20.0 ± 0.8 (at –10 mV)	8	< 0.001
	$V_{1/2}$ (mV)[3]	–24.4 ± 0.6		–18.6 ± 0.9		< 0.001
	k[3]	8.3 ± 0.3		12.7 ± 0.8		< 0.001

[1]Comparison between P6–8 and P16–18 by t-test; [2]obtained from I-V relationships; [3]obtained from G-V relationships.

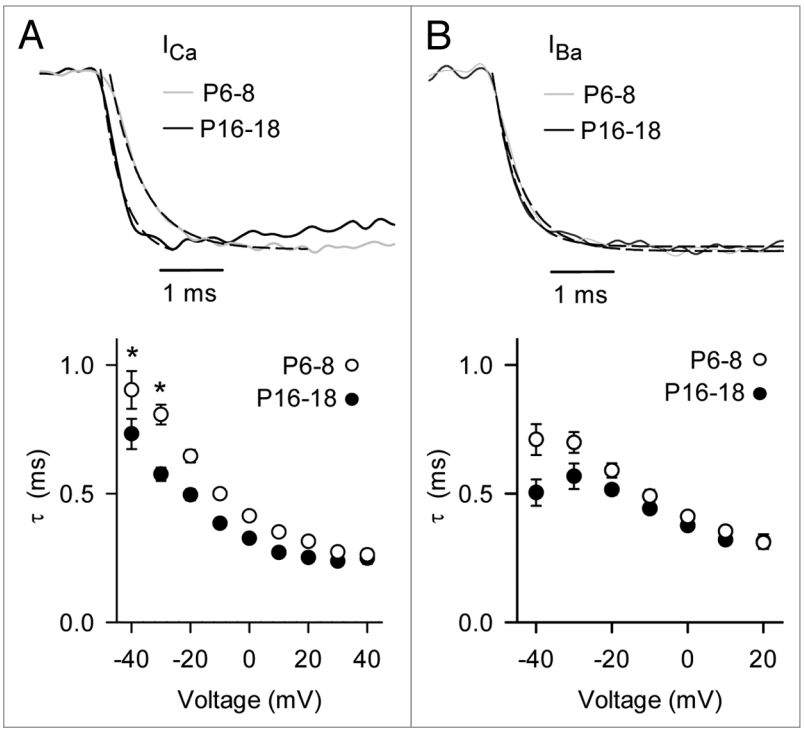

Figure 3. I_{Ca} activation kinetics are faster in mature IHCs than immature IHCs. (**A and B**) Upper panels, representative traces for I_{Ca} and I_{Ba} for P6–8 (gray) or P16–18 (black) IHCs. Currents were evoked by a 15-ms step to –10 mV from a holding potential of –84 mV. Dashed lines represent exponential fits of the current trace. The time constants (τ, ms) for the displayed current traces were: for I_{Ca} (**A**) 0.62 (P6–8) and 0.28 (P16–18); for I_{Ba} (**B**) 0.50 (P6–8) and 0.38 (P16–18). Lower panels, time constants for I_{Ca} (**A**) and I_{Ba} (**B**) were plotted against test voltage. For P6–8, n = 22 for I_{Ca}, 15 for I_{Ba}. For P16–18, n = 11 for I_{Ca}, 15 for I_{Ba}. *p < 0.001 by two-way ANOVA.

immature rat IHCs but not in mature gerbil IHCs is suppressed by high intracellular concentrations (10 mM) of EGTA or BAPTA.[17,18] These results suggest that the Ca^{2+} sensitivity of Ca_v1 CDI may be subject to developmental regulation. To test this, we analyzed the impact of increasing Ca^{2+} buffering strength on CDI in mature and immature mouse IHCs using triple-pulse protocols with varying prepulse voltages. To rapidly buffer incoming Ca^{2+} ions, we used relatively high concentrations (10 mM) of BAPTA in the intracellular recording solution. Since BAPTA (10 mM) does not influence inactivation of I_{Ba} mediated by $Ca_v1.3$,[29] we restricted analysis to I_{Ca} in these experiments. Compared with our standard solution with EGTA (2 mM), the BAPTA-containing solution significantly blunted CDI in immature IHCs across a range of prepulse voltages (up to ~30% between –30 mV and +20 mV, p < 0.05 by two-way ANOVA; **Fig. 7A and B**). Remarkably, this effect of BAPTA was not observed in mature IHCs (p = 0.16 by two-way ANOVA; **Fig. 7A–C**). These effects of BAPTA were not due to altered voltage-dependence of activation, since G-V parameters were not significantly different with BAPTA or low intracellular EGTA (**Table 1**, **Fig. S1**).

The BAPTA-sensitivity of CDI in immature but not mature IHCs suggests that Ca^{2+} elevations that support CDI are not restricted to local Ca^{2+} influx through single channels but rather global Ca^{2+} signals fueled by multiple neighboring channels. In this respect, $Ca_v1.3$ CDI in immature IHCs may be similar mechanistically to CDI of $Ca_v2.1$ channels, which is strongly suppressed by high concentrations of BAPTA or EGTA.[30-34] If so, CDI should increase with channel density in immature IHCs. Consistent with this prediction, p2/p1 ratios decreased (i.e., inactivation increased) with increasing I_{Ca} amplitude (**Fig. 7D**). BAPTA

caused a significant increase in the slope of the p2/p1 vs. I_{Ca} relationship (4×10^{-4} for EGTA vs. 9.5×10^{-4} for BAPTA, $p < 0.03$ by ANCOVA; **Fig. 7D**). These results show that BAPTA increases the current-amplitude dependence of CDI, such that small-amplitude I_{Ca} showed weaker CDI (and BAPTA-sensitivity) than large-amplitude I_{Ca}.

To determine if the sensitivity of CDI to BAPTA in immature IHCs was due to effects of BAPTA on the onset and/or recovery kinetics of I_{Ca} inactivation, we compared these parameters using either 2 mM EGTA or 10 mM BAPTA in the intracellular recording solution. With BAPTA, the onset of inactivation exhibited a double exponential time course as was found for EGTA (**Figs. 5 and 8A–C**). In these experiments, BAPTA did not affect either the slow or fast time constants (τ_{fast} = 48.1 ± 9.2 ms for BAPTA vs. 32.9 ± 3.9 ms for EGTA, $p = 0.06$; τ_{slow} = 1.2 ± 0.3 ms for BAPTA vs. 2.0 ± 0.5 ms for EGTA, $p = 0.07$, both by Mann-Whitney rank sum test; **Fig. 8C**). However, BAPTA significantly decreased the corresponding amplitudes (A_{fast} = 0.15 ± 0.02 for BAPTA vs. 0.25 ± 0.01 for EGTA, $p < 0.001$; A_{slow} = 0.20 ± 0.01 for BAPTA vs. 0.40 ± 0.03 for EGTA, $p < 0.001$, both by Mann-Whitney rank sum test) and increased the available current (Y_0 = 0.66 ± 0.02 for BAPTA vs. 0.34 ± 0.04 for EGTA, $p < 0.001$, by Mann-Whitney rank sum test; **Fig. 8C**). In addition, BAPTA accelerated recovery of I_{Ca} from inactivation (τ = 271.9 ± 28.3 ms for BAPTA vs. 425.9 ± 28.3 ms for EGTA, $p < 0.001$ by t-test; **Fig. 8D–F**). Thus, BAPTA increases $Ca_v1.3$ channel availability in immature IHCs by inhibiting the amount of I_{Ca} inactivation as well as by speeding recovery from CDI. Our results highlight age-dependent differences in the intrinsic properties and modulation of $Ca_v1.3$ channels in mouse IHCs that may be important for the normal function and/or maturation of these cells as sound-transducers in the inner ear.

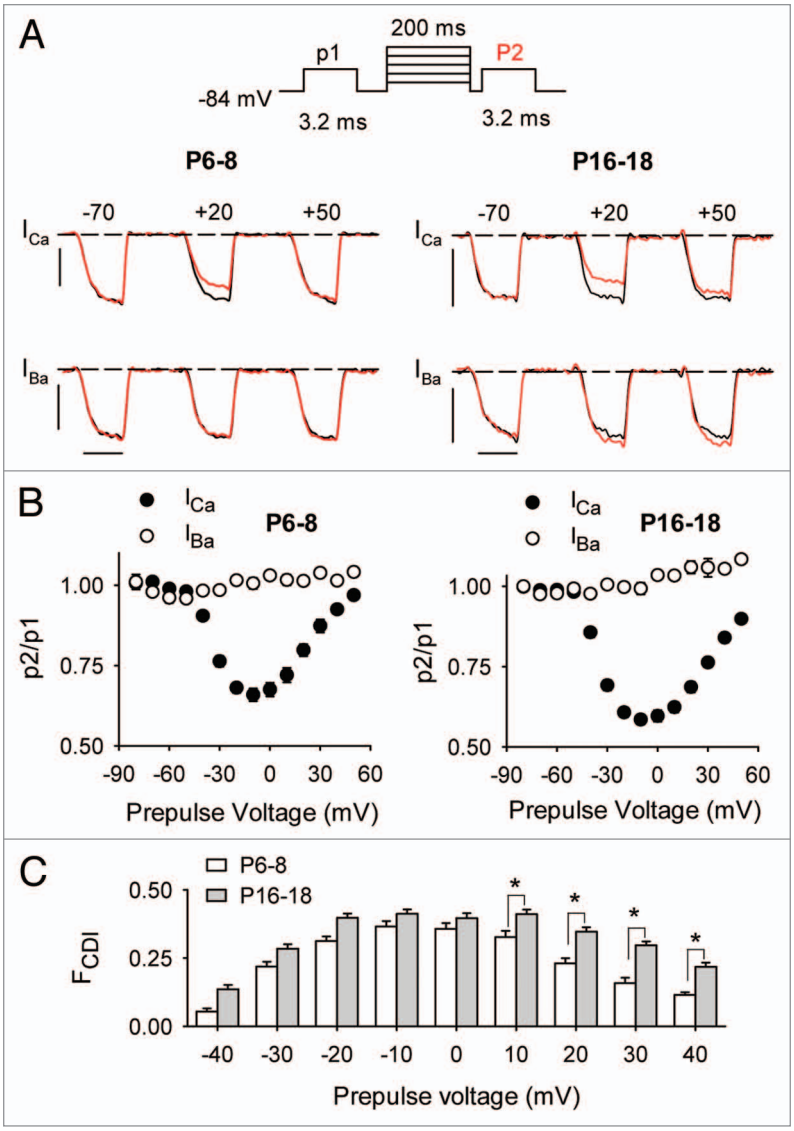

Figure 4. CDI is greater in mature IHCs than immature IHCs. (**A**) Top panel, Voltage protocol in which test currents were evoked by pulses (p1, p2) from –84 to –20 mV (for I_{Ca}) or –30 mV (for I_{Ba}) before and after a 200-ms prepulse to various voltages. Bottom panels, representative traces for I_{Ca} or I_{Ba} recorded in P6–8 or P16–18 mouse IHCs. Currents were evoked by p1 (black) and p2 (red) overlaid for comparison. Scale bars, 0.2 nA (vertical), 2.5 ms (horizontal). (**B**) Inactivation was measured as the ratio of P2/P1 current amplitude and plotted against prepulse voltage. Results are from mouse IHCs from P6–8 (n = 20 for I_{Ca}, n = 6 for I_{Ba}) or P16–18 (n = 18 for I_{Ca}, n = 8 for I_{Ba}). (**C**) CDI was measured as the difference in p2/p1 for I_{Ca} and I_{Ba} (F_{CDI}) and is plotted against prepulse voltage for P6–8 and P16–18 IHCs. *$p < 0.05$ by two-way ANOVA and post-hoc Bonferroni t-test.

Discussion

The aim of the present study was to characterize the biophysical properties of $Ca_v1.3$ channels in mouse IHCs before and after the onset of hearing. While comprehensive analyses of Ca_v1 currents have been performed in auditory hair cells from other species,[17,18,35] details regarding the function and modulation of $Ca_v1.3$ channels in immature and mature mouse IHCs is necessary to understand the sequelae associated with dysregulated Ca^{2+} signaling in mouse models of deafness. Our results indicate that $Ca_v1.3$ channels undergo significant changes in activation and inactivation that may support distinct roles of these channels at different stages of development.

Technical considerations and comparisons with other species. Due to the concentration of Ca^{2+} or Ba^{2+} (5 mM) in our extracellular recording solution and the fact that our recordings were performed at room temperature (~25°C), parameters for I_{Ca} and I_{Ba} activation and inactivation in the present study differ from those expected under physiological conditions (~1.3 mM extracellular Ca^{2+}, ~37°C). In addition to increasing the amplitudes of I_{Ca} and I_{Ba}, the higher than physiological concentration of extracellular permeant ions would cause a positive shift in the half-maximal activation voltage (V_h) due to increased neutralization of cell surface charges.[36] Subsequently, the voltage-dependence of time constants for activation and inactivation

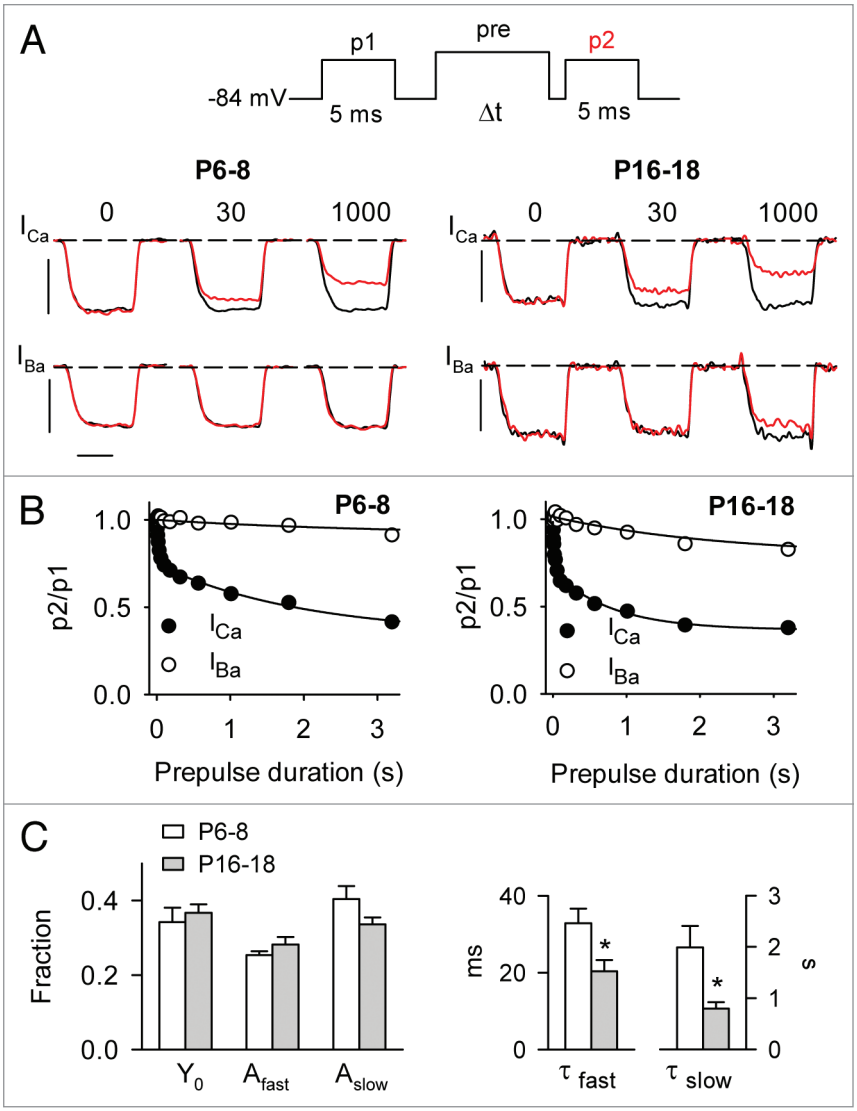

Figure 5. Onset of CDI is faster in mature IHCs than in immature IHCs. (**A**) Top panel, Voltage protocol in which test currents were evoked by pulses (p1, p2) from −84 to −20 mV (for I_{Ca}) or −30 mV (for I_{Ba}) before and after a prepulse to −10 mV of varying durations. Bottom panels, representative traces for I_{Ca} or I_{Ba} recorded in P6–8 or P16–18 mouse IHCs with protocols using the indicated prepulse durations. Currents evoked by p1 (black) and p2 (red) are overlaid for comparison. Scale bars, 0.8 nA (vertical), 2.5 ms (horizontal). (**B**) Onset of inactivation was measured by plotting p2/p1 values against prepulse duration. Smooth line represents fit with a double (I_{Ca}) or single (I_{Ba}) exponential function. For P6–8, curve fit parameters for I_{Ca} were $y_0 = 0.34$, $A_{fast} = 0.25$, $\tau_{fast} = 32.9$ ms, $A_{slow} = 0.40$, $\tau_{slow} = 1990$ ms (n = 22); for I_{Ba}, $y_0 = 0.91$, $A = 56.5$, $\tau = 3108$ ms (n = 8). For P16–18, curve fit parameters for I_{Ca} were $y_0 = 0.37$, $A_{fast} = 0.28$, $\tau_{fast} = 20.4$ ms, $A_{slow} = 0.34$, $\tau_{slow} = 795$ ms (n = 12); for I_{Ba}, $y_0 = 0.79$, $A = 30.1$, $\tau = 2313$ ms (n = 11). (**C**) Average values from exponential fits of I_{Ca} data in (B). *p < 0.02 by Mann-Whitney rank sum test.

should be positively shifted with 5 mM compared with 1.3 mM extracellular Ca^{2+} or Ba^{2+}. However, charge-screening effects of higher divalent concentrations should not influence the voltage-sensitivity of $Ca_v1.3$ activation, which is reflected by the steepness of the G-V curves (*k* from Boltzmann fits).[37,38] Assuming that $Ca_v1.3$ properties in mature and immature IHCs would be equally affected by the increased Ca^{2+} or Ba^{2+} concentration, we would expect our results to accurately report the age-dependent difference, if not the absolute values, pertaining to $Ca_v1.3$ properties.

As shown previously,[17,18] recordings at room temperature (~25°C) would cause smaller Ca_v1 current amplitudes and slower activation and inactivation kinetics than at physiological temperature (~37°C). At the same time, signaling processes that post-translationally alter the intrinsic biophysical properties of $Ca_v1.3$ channels would proceed more rapidly at 37°C than at 25°C. This could be a concern given that Ca_v1 amplitudes in immature IHCs show greater temperature sensitivity (larger Q_{10}) than in mature IHCs in the gerbil.[18] Notably, we observed greater run-up of I_{Ca} upon initiation of whole-cell recordings in immature compared with mature IHCs (**Fig. 1**). Ca_v1 channel run-up has been reported in turtle and frog hair cells[35,39] and in cardiac myocytes (see for example ref. 40). While the underlying mechanisms are not entirely clear, run-up of cardiac Ca_v1 currents is associated with patch rupture in whole-cell recordings and exhibits a rapid (< 5 min) and late (> 10 min) phase, the latter of which is not observed at lower than physiological temperatures.[40] Therefore, our recordings at room temperature may minimize alterations in channel properties resulting from intracellular dialysis.

Our results in mouse IHCs may not be entirely consistent with those reported for gerbil and rat IHCs due to methodological and/or species-related differences. For example, the age-dependent acceleration in I_{Ca} activation kinetics in our study (**Fig. 3**) agrees with results from gerbil IHCs[18] but not rat IHCs, in which I_{Ca} activation was slower after hearing onset than before.[17] In addition, while we found CDI to be greater in mature IHCs than in immature IHCs (**Fig. 4**), there was no such age-related difference in gerbil IHCs,[18] and CDI was actually greater in immature IHCs than in mature IHCs in the rat.[17] Our results regarding the Ca^{2+} buffer-sensitivity of CDI in immature but not in mature mouse IHCs (**Figs. 7 and 8**) are consistent with these previous studies: high concentrations of BAPTA (5 mM) did not affect CDI in mature gerbil IHCs[18] but did significantly suppress CDI in immature rat IHCs.[17] Therefore, the shift in CDI dependence on global Ca^{2+} signals in immature IHCs, to local Ca^{2+} signals in mature IHCs, may be a fundamental feature of IHC development.

Possible mechanisms for developmental alterations in $Ca_v1.3$ function. The properties of Ca_v1 channels are subject to multiple forms of regulation, which could account for the difference in $Ca_v1.3$ properties we noted during mouse IHC development. We

showed previously that the PDZ-domain containing protein harmonin interacts with $Ca_v1.3$ channels in mouse IHCs after hearing onset and inhibits I_{Ba}.[27] In mature mouse IHCs, harmonin enhances proteosomal degradation of $Ca_v1.3$, which could contribute to the age-dependent decrease in I_{Ca} or I_{Ba} current density (**Fig. 2C and D**). A second possibility is related to alternative splicing of the pore-forming $Ca_v1.3$ α_1 subunit ($\alpha_1$1.3), which produces variants that differ in their biophysical properties and modulation.[25,41-47] After hearing onset, there may be an upregulation of $\alpha_1$1.3 variants lacking portions of a C-terminal modulatory domain (CTM), which exhibit decreased current density relative to variants with the intact CTM.[41,48] However, it is also possible that factors regulating the transcription/translation of $Ca_v1.3$ channels could also vary in mouse IHCs with age.

Some CTM-lacking variants exhibit enhanced voltage-dependence of activation and stronger CDI than variants containing the entire CTM.[44] Such variants could account for increased CDI in mature IHCs (**Fig. 4**), but their hyperpolarized activation properties relative to the CTM-containing variants are inconsistent with our findings of weaker voltage-dependent activation of $Ca_v1.3$ currents in mature than in immature mouse IHCs (**Table 1**). Alternative splicing and RNA editing of the calmodulin-binding IQ domain $\alpha_1$1.3 also produce $Ca_v1.3$ variants with limited CDI,[47,49] although the extent to which these variants are present in immature mouse IHCs is unknown. $Ca_v1.3$ channels interact with a variety of regulatory proteins, which may also influence CDI.[50] Rab 3-interacting molecule (RIM2α) inhibits CDI when coexpressed with $Ca_v1.3$ channels in HEK293 cells.[51] RIM2α transcripts were detected in immature but not mature IHCs[51] and so could be responsible for the more moderate CDI in mouse IHCs prior to hearing onset (**Fig. 4**). Other possibilities include Ca^{2+} binding proteins related to calmodulin (CaBPs),[17,21,22] and various synaptic proteins,[52] which also suppress inactivation of $Ca_v1.3$ in heterologous expression systems. Whether such $Ca_v1.3$ modulatory proteins undergo developmental changes in expression remains to be elucidated.

The BAPTA-sensitivity of CDI in immature IHCs (**Figs. 7 and 8**) contrasts with the notion that Ca_v1 channel CDI is largely mediated by local Ca^{2+} influx through single channels.[53] In heterologous systems, $Ca_v1.3$ CDI is spared by high concentrations (10 mM) intracellular BAPTA due to a molecular determinant in the cytoplasmic N-terminal domain of $\alpha_1$1.3 (N-terminal spatial Ca^{2+} transforming element, NSCaTE).[29] Binding of the N-terminal lobe of calmodulin to NSCaTE is thought to alter the Ca^{2+} binding properties of calmodulin such that CDI is determined by rapid local increases in Ca^{2+} that cannot be buffered by BAPTA.[29] Deletion of NSCaTE from $\alpha_1$1.3 transforms the spatial selectivity of $Ca_v1.3$ CDI such that it can be blunted by BAPTA.[29] While $\alpha_1$1.3 splice variants lacking NSCaTE remain to be identified, their presence in immature but not mature IHCs could explain the BAPTA sensitivity of CDI in the former and not the latter. A second possibility relates to the increase in synaptic clustering of $Ca_v1.3$ channels in mouse IHCs after hearing onset.[38,54] In frog auditory hair cells, synchronous multivesicular release occurs even in the presence of 10 mM BAPTA, which is attributed to a role of the ribbon as a barrier for Ca^{2+} diffusion.[55]

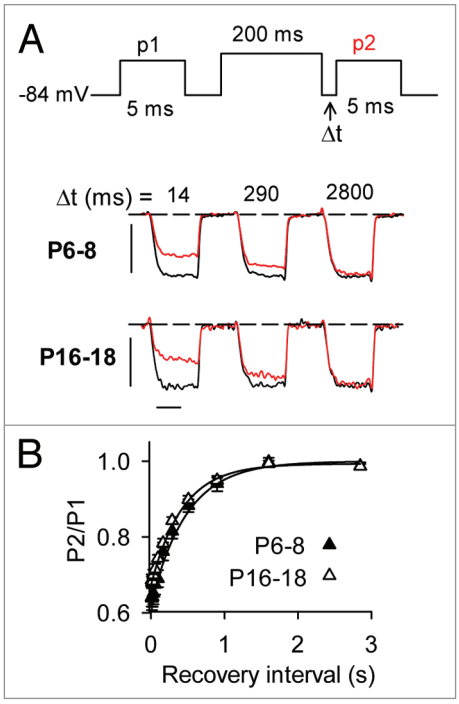

Figure 6. Recovery from CDI does not differ in mature and immature IHCs. (**A**) Top panel, Voltage protocol in which I_{Ca} was evoked by pulses (p1, p2) from –84 to –20 mV before and at variable recovery intervals after a 200-ms prepulse to –10 mV. Bottom panel, representative traces for I_{Ca} recorded in P6–8 or P16–18 mouse IHCs. Currents evoked by p1 (black) and p2 (red) at the indicated recovery intervals are overlaid for comparison. Scale bars, 0.8 nA (vertical), 2.5 ms (horizontal). (**B**) Recovery of I_{Ca} from inactivation was measured by plotting p2/p1 for data obtained as in (**A**) against recovery interval. Data were fit with an exponential function (smooth line). Curve fit parameters were: for P6–8 (n = 19), $y_0 = 0.99$, A; –0.321, $\tau = 425$ ms; for P16–18 (n = 8), $y_0 = 1.0$, $A = -37.8$, $\tau = 486$ ms.

$Ca_v1.3$ channels anchored near the ribbon may therefore be influenced by rapidly accumulating Ca^{2+} nanodomains that promote single-channel CDI in mature IHCs. In contrast, a large fraction of $Ca_v1.3$ channels are extrasynaptically localized prior to hearing onset,[38] where the absence of the ribbon may allow for faster Ca^{2+} diffusion away from open channels and slower elevations in Ca^{2+} that can be buffered by BAPTA.

Physiological significance of age-dependent changes in $Ca_v1.3$ properties and modulation. The distinct properties of $Ca_v1.3$ channels we describe in immature and mature mouse IHCs may support the varying roles of these channels during development. Prior to hearing onset, $Ca_v1.3$ channels mediate spontaneous Ca^{2+}-dependent action potentials,[11] which support exocytosis[12,56] and synaptic activity in the auditory pathway.[57] Raising the concentration of Ca^{2+} in the extracellular recording solution from 1.3 to 5 mM increases the amplitude and accelerates the upstroke and repolarization, and enhances the frequency of the presensory action potentials in mouse IHCs.[56] Therefore, the increased I_{Ca} density and activation and stronger voltage-dependent activation in the immature compared with in mature IHCs (**Fig. 2C and D**; **Table 1**) may be required to maintain the shape and timing of the action potential waveforms. $Ca_v1.3$ Ca^{2+}

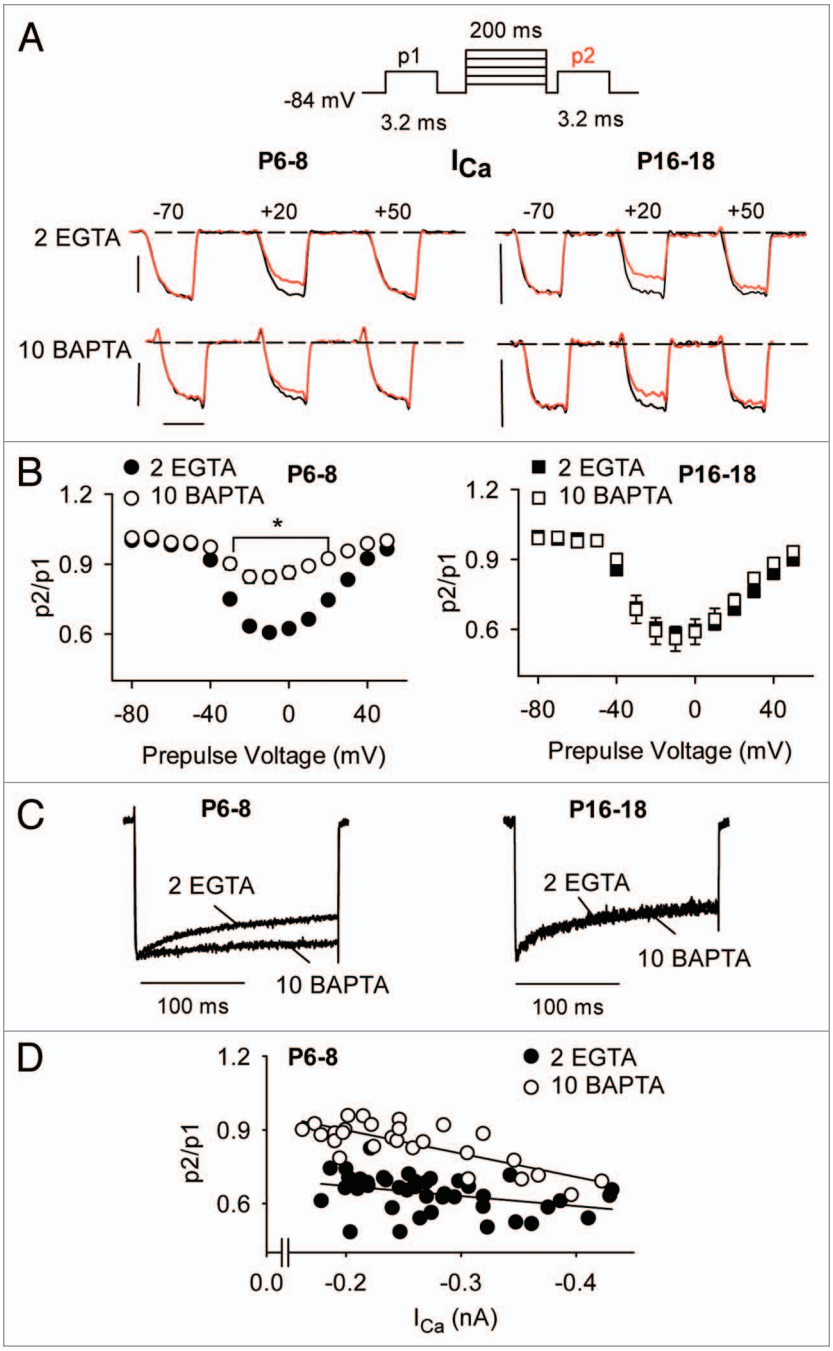

Figure 7. CDI is inhibited by BAPTA in immature IHCs but not mature IHCs. (**A**) Top, Voltage protocol in which test currents were evoked by pulses (p1, p2) from –84 to –20 mV before and after a 200-ms prepulse to various voltages. Bottom, Representative traces for I_{Ca} recorded in P6–8 or P16–18 mouse IHCs with protocols using the indicated prepulse voltages. Intracellular recording solution contains 2 mM EGTA or 10 mM BAPTA. Currents evoked by p1 (black) and p2 (red) are overlaid for comparison. Scale bars, 0.2 nA (vertical), 2.5 ms (horizontal). (**B**) p2/p1 was plotted against prepulse voltage for P6–8 (n = 20 for 2 EGTA, n = 25 for 10 BAPTA) and P16–18 (n = 18 for 2 EGTA, n = 8 for BAPTA). *p < 0.05 for EGTA vs. BAPTA, by two-way ANOVA and Bonferroni t-test. (**C**) Representative normalized current traces obtained with 2 EGTA or 10 BAPTA. I_{Ca} was evoked by a 200-ms test pulse to –10 from –84 mV. (**D**) For P6–8 IHCs, p2/p1 ratios were plotted against I_{Ca} amplitude for 2 EGTA or 10 BAPTA. Lines represent fits by linear regression.

influx enhances repolarization of the action potential through coupling to the activation of SK Ca^{2+} activation K^+ channels.[58] Based on the ability of BAPTA to suppress $Ca_v1.3$-dependent activation of SK channels, $Ca_v1.3$ channels may be localized ~40 nm from SK channels.[58] This is in contrast to the tighter coupling of nicotinic acetylcholine receptors (~13 nm distance),[58] which also conduct Ca^{2+} that activates SK channels.[13,59] In this context, the reduced CDI prior to hearing onset (**Fig. 4**) would allow for more prolonged Ca^{2+} signals that support SK channel activation and efficient Ca^{2+} spiking. In addition, sustained I_{Ca} in immature IHCs may support activity-dependent gene transcription, a hallmark function of Ca_v1 channels in the central nervous system.[60] $Ca_v1.3$ channels are required for normal levels of BK K^+ channel transcription in mouse IHCs,[16] and BK channel expression in muscle is regulated by the Ca^{2+}-dependent gene transcription factor, nuclear factor of activated T-cells (NFAT3).[61] Future studies analyzing gene expression differences in mature and immature IHCs would help identify Ca^{2+}-regulated transcripts that may be important for IHC development.

In mature IHCs, the developmental enhancement of $Ca_v1.3$ activation kinetics (**Fig. 3**) and CDI (**Fig. 4**) may improve the temporal aspects of sound coding. In paired, pre- and postsynaptic recording at the IHC synapse, faster $Ca_v1.3$ activation correlates with decreased latency of postsynaptic responses,[62] which supports the ability of auditory nerve fibers to fire at particular times during low-frequency stimuli (phase-locking).[63] While $Ca_v1.3$ CDI would be expected to limit exocytosis by restricting Ca^{2+} influx, CDI is expected to contribute modestly to depression at the IHC synapse.[62,64,65] Rather, CDI may help shape Ca^{2+} signals required for appropriate rates of vesicle replenishment at the ribbon[64,65] and/or help limit Ca^{2+} loads that could provoke metabolic stress.

In summary, we have described key functional distinctions in the properties of $Ca_v1.3$ channels in immature and mature mouse IHCs. An understanding of how these developmental differences in $Ca_v1.3$ Ca^{2+} signals contribute to the maturation and function of IHCs in the auditory pathway remains an important challenge for future studies.

Materials and Methods

Ethical approval. All procedures were approved by the Institutional Animal Care and Use Committee at the University of Iowa in accordance with National Institutes of Health guidelines.

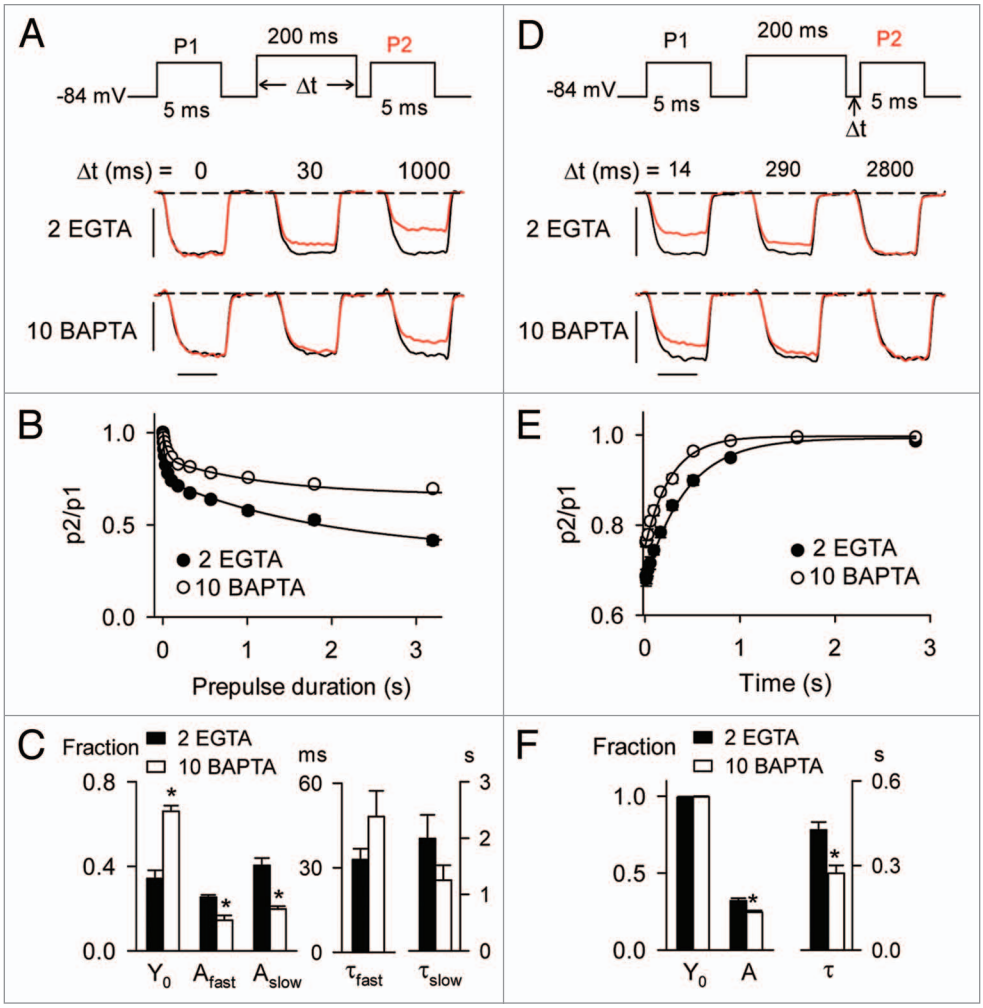

Figure 8. BAPTA slows the onset and accelerates recovery of CDI in immature IHCs. (**A**) Voltage protocol and representative p1 and p2 current traces for I_{Ca} with the indicated prepulse durations. Scale bars, 0.2 nA (vertical), 2.5 ms (horizontal). (**B**) Graph shows data plotted as in **Figure 4B** for I_{Ca} recorded with 2 EGTA (n = 22) or 10 BAPTA (n = 14). Smooth line represents double exponential curve fit (for 10 BAPTA, $y_0 = 0.66$, $A_{fast} = 0.14$, $\tau_{fast} = 48.1$ ms, $A_{slow} = 0.20$, $\tau_{slow} = 1251$ ms; see **Figure 4B** for parameters for 2 EGTA). (**C**) Average parameters for exponential fits of data in (**B**).*p < 0.001 by Mann-Whitney rank sum test. (**D**) Voltage protocol and representative p1 and p2 current traces for I_{Ca} with the indicated recovery intervals. Scale bars, 0.2 nA (vertical), 2.5 ms (horizontal). (**E**) Graph shows data plotted as in **Figure 5B** for I_{Ca} recorded with 2 EGTA (n = 8) or 10 BAPTA (n = 14). Smooth line represents exponential curve fit ($y_0 = 1.0$, $A = -0.25$, $\tau = 271$ ms see **Fig. 5B** for parameters for 2 EGTA). (**F**) Average parameters for exponential fits of data in (**E**). *p < 0.001 by t- test.

Preparation of mouse cochlear tissue. C57bl/6 mice (Harlan Laboratories; P6–8 or P16–18 males or females) were euthanized with ketamine (100 mg/kg) and xylazine (9 mg/kg), the skull was opened, and the temporal bones were dissected out and immersed in dissection solution (MEM/Glutamax-1 (Invitrogen) supplemented with 10 mM HEPES) which was preincubated at 37°C in a humidified incubator with 5% CO_2. The apical turn was dissected in fresh dissection solution and the spiral ligament removed. The tissue was then secured under a glass pin on a 15 mm round coverslip in dissection solution and incubated for 2–5 h at 37°C in a humidified incubator with 5% CO_2 prior to recording.

Electrophysiological recordings. IHCs in the apical cochlear turn were visualized on an upright microscope (BX51WI, Olympus) with a 40× water-immersion objective with DIC optics. The basolateral membrane of IHCs was subject to whole-cell patch clamp recording with electrodes pulled from thick-walled borosilicate glass capillaries (1B150F, Warner Instruments). Before recording, the viability of the IHCs was confirmed by the following morphological features: uniform cell shape with a narrow neck, basal location of the nucleus, membrane birefringence, and intact stereocilia. The internal solution contained (in mM): 100 Cs-gluconate, 30 TEA-Cl, 1 $MgCl_2$, 4 MgATP, 0.3GTP, 5 HEPES and 2 EGTA; pH was adjusted to 7.35 with CsOH; osmolarity~305 mOsm. In some experiments, 10 mM BAPTA was substituted for 2 EGTA and Cs-gluconate was reduced to 92 mM. External solution contained (in mM): 105 NaCl, 2.8 KCl, 3 CsCl, 35 TEA-Cl, 5 $CaCl_2$ or $BaCl_2$, 1 $MgCl_2$, 10 glucose, and 10 HEPES supplemented with MEM Vitamins and Amino Acids at 1X; pH was adjusted to 7.4 with TEA-OH; osmolarity~310 mOsm. Under these conditions, the

free intracellular Ca^{2+} was estimated to be less than 0.5 nM (with 2 mM intracellular EGTA) or less than 0.1 nM (with 10 mM intracellular BAPTA). On the day of recording, 4-aminopyridine (10 mM), apamin (0.3 mM) and TTX (0.5 mM, for P6–8 IHCs) were added to the external solution. Electrode resistances were 3–5 MΩ in the external solution. Data were acquired at room temperature with a HEKA EPC-10 amplifier controlled by Patchmaster software (HEKA Elektronik). Leak subtraction was done online with a P/8 protocol. Series resistance was compensated with the patch clamp circuitry (50–70%); average uncompensated series resistance was 9.64 ± 0.38 (n = 121). Currents were low-pass filtered at 5 kHz and sampled at 20 kHz. Voltages were not corrected for the liquid junction potential of –7 mV in the external recording solution.

Electrophysiological data were analyzed with custom routines in IgorPro software (Wavemetrics). Current-voltage (I-V) relationships were fit with the equation: $I = [G_{max} (V - V_{rev})]/ [1 + exp [(V_h - V)/k]]$, where I is the current, G_{max} is maximum chord conductance, V is voltage, V_{rev} is reversal potential, V_h is half-maximal activation voltage, and k is the slope factor. Conductance-voltage relationships were fit with the equation; $G/G_{max} = 1/ [1 + exp [(V_h - V)/k]]$. Time constants for activation and parameters for recovery from inactivation were obtained by fitting with the equation: $I(t) = y_o + A[exp (-t/\tau)]$, where $I(t)$ is current at time = t, y_0 is the offset (asymptote), A is the amplitude, and τ is the time constant. The onset of I_{Ca} inactivation was fit with a double exponential function: $I(t) = y_0 + A_{fast} [exp (-t/\tau_{fast})] + A_{slow} [exp (-t/\tau_{slow})]$ where $I(t)$ is current at time = t, y_0 is the offset (asymptote), A_{fast} and A_{slow} are the amplitudes, and τ_{fast} and τ_{slow} are the time constants. Average data are expressed as mean ± SEM. Statistical comparisons were done as indicated using SigmaPlot software (Systat).

Disclosure of Potential Conflicts of Interest

No potential conflicts of interest were disclosed.

Acknowledgments

Support was provided by the NIH (DC009433, HL087120 to A.L. and DC010362 for support of the Iowa Center for Molecular Auditory Neuroscience) and a Carver Research Program of Excellence Award to A.L.

Supplemental Material

Supplemental materials may be found here:
http://www.landesbioscience.com/journals/channels/article/24104

References

1. Ertel EA, Campbell KP, Harpold MM, Hofmann F, Mori Y, Perez-Reyes E, et al. Nomenclature of voltage-gated calcium channels. Neuron 2000; 25:533-5; PMID:10774722; http://dx.doi.org/10.1016/S0896-6273(00)81057-0
2. Hell JW, Westenbroek RE, Warner C, Ahlijanian MK, Prystay W, Gilbert MM, et al. Identification and differential subcellular localization of the neuronal class C and class D L-type calcium channel α_1 subunits. J Cell Biol 1993; 123:949-62; PMID:8227151; http://dx.doi.org/10.1083/jcb.123.4.949
3. Finkbeiner S, Greenberg ME. Ca^{2+} channel-regulated neuronal gene expression. J Neurobiol 1998; 37:171-89; PMID:9777740; http://dx.doi.org/10.1002/(SICI)1097-4695(199810)37:1<171::AID-NEU13>3.0.CO;2-H
4. Dunlap K, Luebke JI, Turner TJ. Exocytotic Ca^{2+} channels in mammalian central neurons. Trends Neurosci 1995; 18:89-98; PMID:7537420; http://dx.doi.org/10.1016/0166-2236(95)93882-X
5. Westenbroek RE, Hell JW, Warner C, Dubel SJ, Snutch TP, Catterall WA. Biochemical properties and subcellular distribution of an N-type calcium channel α_1 subunit. Neuron 1992; 9:1099-115; PMID:1334419; http://dx.doi.org/10.1016/0896-6273(92)90069-P
6. Westenbroek RE, Sakurai T, Elliott EM, Hell JW, Starr TV, Snutch TP, et al. Immunochemical identification and subcellular distribution of the α_{1A} subunits of brain calcium channels. J Neurosci 1995; 15:6403-18; PMID:7472404
7. Fuchs PA, Evans MG, Murrow BW. Calcium currents in hair cells isolated from the cochlea of the chick. J Physiol 1990; 429:553-68; PMID:1703574
8. Roberts WM, Jacobs RA, Hudspeth AJ. Colocalization of ion channels involved in frequency selectivity and synaptic transmission at presynaptic active zones of hair cells. J Neurosci 1990; 10:3664-84; PMID:1700083
9. Platzer J, Engel J, Schrott-Fischer A, Stephan K, Bova S, Chen H, et al. Congenital deafness and sinoatrial node dysfunction in mice lacking class D L-type Ca^{2+} channels. Cell 2000; 102:89-97; PMID:10929716; http://dx.doi.org/10.1016/S0092-8674(00)00013-1
10. Dou H, Vazquez AE, Namkung Y, Chu H, Cardell EL, Nie L, et al. Null mutation of α1D Ca^{2+} channel gene results in deafness but no vestibular defect in mice. J Assoc Res Otolaryngol 2004; 5:215-26; PMID:15357422; http://dx.doi.org/10.1007/s10162-003-4020-3
11. Brandt A, Striessnig J, Moser T. CaV1.3 channels are essential for development and presynaptic activity of cochlear inner hair cells. J Neurosci 2003; 23:10832-40; PMID:14645476
12. Beutner D, Moser T. The presynaptic function of mouse cochlear inner hair cells during development of hearing. J Neurosci 2001; 21:4593-9; PMID:11425887
13. Glowatzki E, Fuchs PA. Cholinergic synaptic inhibition of inner hair cells in the neonatal mammalian cochlea. Science 2000; 288:2366-8; PMID:10875922; http://dx.doi.org/10.1126/science.288.5475.2366
14. Johnson SL, Marcotti W, Kros CJ. Increase in efficiency and reduction in Ca^{2+} dependence of exocytosis during development of mouse inner hair cells. J Physiol 2005; 563:177-91; PMID:15613377; http://dx.doi.org/10.1113/jphysiol.2004.074740
15. Kros CJ, Ruppersberg JP, Rüsch A. Expression of a potassium current in inner hair cells during development of hearing in mice. Nature 1998; 394:281-4; PMID:9685158; http://dx.doi.org/10.1038/28401
16. Nemzou N RM, Bulankina AV, Khimich D, Giese A, Moser T. Synaptic organization in cochlear inner hair cells deficient for the $Ca_V1.3$ (alpha1D) subunit of L-type Ca^{2+} channels. Neuroscience 2006; 141:1849-60; PMID:16828974; http://dx.doi.org/10.1016/j.neuroscience.2006.05.057
17. Grant L, Fuchs P. Calcium- and calmodulin-dependent inactivation of calcium channels in inner hair cells of the rat cochlea. J Neurophysiol 2008; 99:2183-93; PMID:18322004; http://dx.doi.org/10.1152/jn.01174.2007
18. Johnson SL, Marcotti W. Biophysical properties of CaV1.3 calcium channels in gerbil inner hair cells. J Physiol 2008; 586:1029-42; PMID:18174213; http://dx.doi.org/10.1113/jphysiol.2007.145219
19. Liang H, DeMaria CD, Erickson MG, Mori MX, Alseikhan BA, Yue DT. Unified mechanisms of Ca^{2+} regulation across the Ca^{2+} channel family. Neuron 2003; 39:951-60; PMID:12971895; http://dx.doi.org/10.1016/S0896-6273(03)00560-9
20. Christel C, Lee A. Ca2+-dependent modulation of voltage-gated Ca2+ channels. Biochim Biophys Acta 2012; 1820:1243-52; PMID:22223119; http://dx.doi.org/10.1016/j.bbagen.2011.12.012
21. Yang PS, Alseikhan BA, Hiel H, Grant L, Mori MX, Yang W, et al. Switching of Ca^{2+}-dependent inactivation of $Ca_{(v)}1.3$ channels by calcium binding proteins of auditory hair cells. J Neurosci 2006; 26:10677-89; PMID:17050707; http://dx.doi.org/10.1523/JNEUROSCI.3236-06.2006
22. Cui G, Meyer AC, Calin-Jageman I, Neef J, Haeseleer F, Moser T, et al. Ca2+-binding proteins tune Ca2+-feedback to Cav1.3 channels in mouse auditory hair cells. J Physiol 2007; 585:791-803; PMID:17947313; http://dx.doi.org/10.1113/jphysiol.2007.142307
23. Tiaho F, Nargeot J, Richard S. Repriming of L-type calcium currents revealed during early whole-cell patch-clamp recordings in rat ventricular cells. J Physiol 1993; 463:367-89; PMID:8246188
24. Cota G, Stefani E. Saturation of calcium channels and surface charge effects in skeletal muscle fibres of the frog. J Physiol 1984; 351:135-54; PMID:6086902
25. Safa P, Boulter J, Hales TG. Functional properties of $Ca_v1.3$ (alpha1D) L-type Ca^{2+} channel splice variants expressed by rat brain and neuroendocrine GH3 cells. J Biol Chem 2001; 276:38727-37; PMID:11514547; http://dx.doi.org/10.1074/jbc.M103724200
26. Wang CL. A note on Ca2+ binding to calmodulin. Biochem Biophys Res Commun 1985; 130:426-30; PMID:4026838; http://dx.doi.org/10.1016/0006-291X(85)90434-6
27. Gregory FD, Bryan KE, Pangršic T, Calin-Jageman IE, Moser T, Lee A. Harmonin inhibits presynaptic Cav1.3 Ca^{2+} channels in mouse inner hair cells. Nat Neurosci 2011; 14:1109-11; PMID:21822269; http://dx.doi.org/10.1038/nn.2895
28. Tadross MR, Dick IE, Yue DT. Mechanism of local and global Ca^{2+} sensing by calmodulin in complex with a Ca2+ channel. Cell 2008; 133:1228-40; PMID:18585356; http://dx.doi.org/10.1016/j.cell.2008.05.025
29. Dick IE, Tadross MR, Liang H, Tay LH, Yang W, Yue DT. A modular switch for spatial Ca2+ selectivity in the calmodulin regulation of CaV channels. Nature 2008; 451:830-4; PMID:18235447; http://dx.doi.org/10.1038/nature06529

30. Lee A, Scheuer T, Catterall WA. Ca^{2+}/calmodulin-dependent facilitation and inactivation of P/Q-type Ca^{2+} channels. J Neurosci 2000; 20:6830-8; PMID:10995827
31. Lee A, Wong ST, Gallagher D, Li B, Storm DR, Scheuer T, et al. Ca^{2+}/calmodulin binds to and modulates P/Q-type calcium channels. Nature 1999; 399:155-9; PMID:10335845; http://dx.doi.org/10.1038/20194
32. DeMaria CD, Soong TW, Alseikhan BA, Alvania RS, Yue DT. Calmodulin bifurcates the local Ca^{2+} signal that modulates P/Q-type Ca^{2+} channels. Nature 2001; 411:484-9; PMID:11373682; http://dx.doi.org/10.1038/35078091
33. Kreiner L, Lee A. Endogenous and exogenous Ca^{2+} buffers differentially modulate Ca^{2+}-dependent inactivation of $Ca_{(v)}2.1$ Ca^{2+} channels. J Biol Chem 2006; 281:4691-8; PMID:16373336; http://dx.doi.org/10.1074/jbc.M511971200
34. Soong TW, DeMaria CD, Alvania RS, Zweifel LS, Liang MC, Mittman S, et al. Systematic identification of splice variants in human P/Q-type channel $\alpha_1(2.1)$ subunits: implications for current density and Ca^{2+}-dependent inactivation. J Neurosci 2002; 22:10142-52; PMID:12451115
35. Schnee ME, Ricci AJ. Biophysical and pharmacological characterization of voltage-gated calcium currents in turtle auditory hair cells. J Physiol 2003; 549:697-717; PMID:12740421; http://dx.doi.org/10.1113/jphysiol.2002.037481
36. Hille B, ed. Ionic channels of excitable membranes, 2nd ed. Sunderland, MA: Sinauer Associates Inc., 1992
37. Rodríguez-Contreras A, Yamoah EN. Effects of permeant ion concentrations on the gating of L-type Ca2+ channels in hair cells. Biophys J 2003; 84:3457-69; PMID:12719271; http://dx.doi.org/10.1016/S0006-3495(03)70066-6
38. Zampini V, Johnson SL, Franz C, Lawrence ND, Münkner S, Engel J, et al. Elementary properties of CaV1.3 Ca(2+) channels expressed in mouse cochlear inner hair cells. J Physiol 2010; 588:187-99; PMID:19917569; http://dx.doi.org/10.1113/jphysiol.2009.181917
39. Martini M, Rossi ML, Rubbini G, Rispoli G. Calcium currents in hair cells isolated from semicircular canals of the frog. Biophys J 2000; 78:1240-54; PMID:10692313; http://dx.doi.org/10.1016/S0006-3495(00)76681-1
40. Yamaoka K, Yuki T, Kawase K, Munemori M, Seyama I. Temperature-sensitive intracellular Mg^{2+} block of L-type Ca2+ channels in cardiac myocytes. Am J Physiol Heart Circ Physiol 2002; 282:H1092-101; PMID:11834508
41. Tan BZ, Jiang F, Tan MY, Yu D, Huang H, Shen Y, et al. Functional characterization of alternative splicing in the C terminus of L-type CaV1.3 channels. J Biol Chem 2011; 286:42725-35; PMID:21998309; http://dx.doi.org/10.1074/jbc.M111.265207
42. Xu W, Lipscombe D. Neuronal Ca(V)1.3α(1) L-type channels activate at relatively hyperpolarized membrane potentials and are incompletely inhibited by dihydropyridines. J Neurosci 2001; 21:5944-51; PMID:11487617
43. Klugbauer N, Welling A, Specht V, Seisenberger C, Hofmann F. L-type Ca^{2+} channels of the embryonic mouse heart. Eur J Pharmacol 2002; 447:279-84; PMID:12151019; http://dx.doi.org/10.1016/S0014-2999(02)01850-2
44. Lieb A, Scharinger A, Sartori S, Sinnegger-Brauns MJ, Striessnig J. Structural determinants of CaV1.3 L-type calcium channel gating. Channels (Austin) 2012; 6:197-205; PMID:22760075; http://dx.doi.org/10.4161/chan.21002
45. Bock G, Gebhart M, Scharinger A, Jangsangthong W, Busquet P, Poggiani C, et al. Functional properties of a newly identified C-terminal splice variant of $Ca_v1.3$ L-type Ca^{2+} channels. J Biol Chem 2011; 286:42736-48; PMID:21998310; http://dx.doi.org/10.1074/jbc.M111.269951
46. Koschak A, Reimer D, Huber I, Grabner M, Glossmann H, Engel J, et al. α_{1D} ($Ca_v1.3$) subunits can form l-type Ca^{2+} channels activating at negative voltages. J Biol Chem 2001; 276:22100-6; PMID:11285265; http://dx.doi.org/10.1074/jbc.M101469200
47. Shen Y, Yu D, Hiel H, Liao P, Yue DT, Fuchs PA, et al. Alternative splicing of the Ca(v)1.3 channel IQ domain, a molecular switch for Ca^{2+}-dependent inactivation within auditory hair cells. J Neurosci 2006; 26:10690-9; PMID:17050708; http://dx.doi.org/10.1523/JNEUROSCI.2093-06.2006
48. Singh A, Gebhart M, Fritsch R, Sinnegger-Brauns MJ, Poggiani C, Hoda JC, et al. Modulation of voltage- and Ca2+-dependent gating of CaV1.3 L-type calcium channels by alternative splicing of a C-terminal regulatory domain. J Biol Chem 2008; 283:20733-44; PMID:18482979; http://dx.doi.org/10.1074/jbc.M802254200
49. Huang H, Tan BZ, Shen Y, Tao J, Jiang F, Sung YY, et al. RNA editing of the IQ domain in Ca(v)1.3 channels modulates their Ca^{2+}-dependent inactivation. Neuron 2012; 73:304-16; PMID:22284185; http://dx.doi.org/10.1016/j.neuron.2011.11.022
50. Calin-Jageman I, Lee A. Ca(v)1 L-type Ca^{2+} channel signaling complexes in neurons. J Neurochem 2008; 105:573-83; PMID:18266933; http://dx.doi.org/10.1111/j.1471-4159.2008.05286.x
51. Gebhart M, Juhasz-Vedres G, Zuccotti A, Brandt N, Engel J, Trockenbacher A, et al. Modulation of Cav1.3 Ca2+ channel gating by Rab3 interacting molecule. Mol Cell Neurosci 2010; 44:246-59; PMID:20363327; http://dx.doi.org/10.1016/j.mcn.2010.03.011
52. Song H, Nie L, Rodriguez-Contreras A, Sheng ZH, Yamoah EN. Functional interaction of auxiliary subunits and synaptic proteins with Ca(v)1.3 may impart hair cell Ca^{2+} current properties. J Neurophysiol 2003; 89:1143-9; PMID:12574487; http://dx.doi.org/10.1152/jn.00482.2002
53. Yue DT, Backx PH, Imredy JP. Calcium-sensitive inactivation in the gating of single calcium channels. Science 1990; 250:1735-8; PMID:2176745; http://dx.doi.org/10.1126/science.2176745
54. Brandt A, Khimich D, Moser T. Few CaV1.3 channels regulate the exocytosis of a synaptic vesicle at the hair cell ribbon synapse. J Neurosci 2005; 25:11577-85; PMID:16354915; http://dx.doi.org/10.1523/JNEUROSCI.3411-05.2005
55. Graydon CW, Cho S, Li GL, Kachar B, von Gersdorff H. Sharp Ca^{2+} nanodomains beneath the ribbon promote highly synchronous multivesicular release at hair cell synapses. J Neurosci 2011; 31:16637-50; PMID:22090491; http://dx.doi.org/10.1523/JNEUROSCI.1866-11.2011
56. Marcotti W, Johnson SL, Rusch A, Kros CJ. Sodium and calcium currents shape action potentials in immature mouse inner hair cells. J Physiol 2003; 552:743-61; PMID:12937295; http://dx.doi.org/10.1113/jphysiol.2003.043612
57. Tritsch NX, Rodríguez-Contreras A, Crins TT, Wang HC, Borst JG, Bergles DE. Calcium action potentials in hair cells pattern auditory neuron activity before hearing onset. Nat Neurosci 2010; 13:1050-2; PMID:20676105; http://dx.doi.org/10.1038/nn.2604
58. Marcotti W, Johnson SL, Kros CJ. A transiently expressed SK current sustains and modulates action potential activity in immature mouse inner hair cells. J Physiol 2004; 560:691-708; PMID:15331671; http://dx.doi.org/10.1113/jphysiol.2004.072868
59. Oliver D, Klöcker N, Schuck J, Baukrowitz T, Ruppersberg JP, Fakler B. Gating of Ca^{2+}-activated K^+ channels controls fast inhibitory synaptic transmission at auditory outer hair cells. Neuron 2000; 26:595-601; PMID:10896156; http://dx.doi.org/10.1016/S0896-6273(00)81197-6
60. Ma H, Cohen S, Li B, Tsien RW. Exploring the dominant role of Cav1 channels in signalling to the nucleus. Biosci Rep 2012; 33; PMID:23088728; http://dx.doi.org/10.1042/BSR20120099
61. Layne JJ, Werner ME, Hill-Eubanks DC, Nelson MT. NFATc3 regulates BK channel function in murine urinary bladder smooth muscle. Am J Physiol Cell Physiol 2008; 295:C611-23; PMID:18579799; http://dx.doi.org/10.1152/ajpcell.00435.2007
62. Goutman JD. Transmitter release from cochlear hair cells is phase locked to cyclic stimuli of different intensities and frequencies. J Neurosci 2012; 32:17025-35a; PMID:23175853; http://dx.doi.org/10.1523/JNEUROSCI.0457-12.2012
63. Rose JE, Brugge JF, Anderson DJ, Hind JE. Phase-locked response to low-frequency tones in single auditory nerve fibers of the squirrel monkey. J Neurophysiol 1967; 30:769-93; PMID:4962851
64. Moser T, Beutner D. Kinetics of exocytosis and endocytosis at the cochlear inner hair cell afferent synapse of the mouse. Proc Natl Acad Sci U S A 2000; 97:883-8; PMID:10639174; http://dx.doi.org/10.1073/pnas.97.2.883
65. Cho S, Li GL, von Gersdorff H. Recovery from short-term depression and facilitation is ultrafast and Ca^{2+} dependent at auditory hair cell synapses. J Neurosci 2011; 31:5682-92; PMID:21490209; http://dx.doi.org/10.1523/JNEUROSCI.5453-10.2011